AIP | Journal of Applied Physics

The abnormal electrical and optical properties in Na and Ni codoped BiFeO3 nanoparticles

Xunling Xu, Weifang Liu, Hong Zhang, Minchen Guo, Ping Wu, Shouyu Wang, Ju Gao, and Guanghui Rao

Citation: Journal of Applied Physics **117**, 174106 (2015); doi: 10.1063/1.4919822
View online: http://dx.doi.org/10.1063/1.4919822
View Table of Contents: http://scitation.aip.org/content/aip/journal/jap/117/17?ver=pdfcov
Published by the AIP Publishing

JOURNAL OF APPLIED PHYSICS **117**, 174106 (2015)

The abnormal electrical and optical properties in Na and Ni codoped $BiFeO_3$ nanoparticles

Xunling Xu,[1] Weifang Liu,[1,a)] Hong Zhang,[1] Minchen Guo,[1] Ping Wu,[1] Shouyu Wang,[2,3,a)] Ju Gao,[3] and Guanghui Rao[4]
[1]*Tianjin Key Laboratory of Low Dimensional Materials Physics and Preparing Technology, School of Science, Tianjin University, Tianjin 300072, China*
[2]*College of Physics and Materials Science, Tianjin Normal University, Tianjin 300074, China*
[3]*Department of Physics, The University of Hong Kong, Pokfulam Road, Hong Kong*
[4]*Department of Information Materials Science and Engineering, Guilin University of Electronic Technology, Guilin 541004, Guangxi, China*

(Received 12 February 2015; accepted 25 April 2015; published online 6 May 2015)

$Bi_{0.97}Na_{0.03}Fe_{1-x}Ni_xO_3$ ($x = 0$, 0.005, 0.01, 0.015) nanoparticles are prepared via a sol-gel method. Weak ferromagnetism and exchange bias phenomenon without field cooling are observed in the samples. The oxygen vacancy concentration and leakage current density are increased with increasing the Ni content. However, with the increase of Ni content, the band gap of $Bi_{0.97}Na_{0.03}Fe_{1-x}Ni_xO_3$ nanoparticles first decreases and then increases. To explain the abnormal phenomenon, the interplay of oxygen vacancy donor and hole acceptor is analyzed and a phenomenological qualitative model based on the electronic energy band is proposed. Additionally, the threshold switching behavior appears in $Bi_{0.97}Na_{0.03}Fe_{1-x}Ni_xO_3$ samples with $x = 0.01$, 0.015 and the effect is qualitatively explained by introducing a conducting channel model based on the high-density mobile charges. [http://dx.doi.org/10.1063/1.4919822]

INTRODUCTION

Magnetoelectric multiferroics have attracted extensive studies in recent years, due to their potential applications in data storage, sensors, memory devices, and spintronic devices.[1–4] The multiferroic materials show both ferroelectric and ferromagnetic (or antiferromagnetic) ordering within a single phase. However, these kinds of materials are rare in ABO_3 type of perovskite materials, since for being simultaneously ferroelectric and ferromagnetic the material requires empty and partially filled transition metal d-orbitals, respectively, which are mutually exclusive properties.[1] Among these rare ABO_3 type of perovskite multiferroic materials, $BiFeO_3$ is the most promising for practical applications, as it possesses high ferroelectric Curie temperature ($T_C \sim 1103$ K) and high G-type antiferromagnetic Néel temperature ($T_N \sim 643$ K).[5] Unfortunately, the antiferromagnetic nature and modulated spin spiral structure do not provide a net magnetization in bulk $BiFeO_3$ which restrict multiferroic property.[6] In addition, $BiFeO_3$ bulks suffer from large leakage current density, which also prevents these materials from essential polarization performances.[7] Accordingly, numerous attempts have been devoted to overcoming these obstacles.

Recent studies based on $BiFeO_3$ nanowires and nanoparticles show weak ferromagnetism due to significant size effect on the modification of magnetic properties.[8,9] Additionally, the extensive investigations have focused on substitution of rare-earth or alkaline earth elements at A-site, B-site, or A-B-site of $BiFeO_3$.[10–12] There are many reports on the rare-earth doped $BiFeO_3$, such as La, Gd, Sm, which are known to stabilize the single phase of $BiFeO_3$, reduce the leakage current and improve the magnetic properties.[13–15] Also, it has been reported that reduced leakage current and weak ferromagnetism were observed in $BiFeO_3$ nanoparticles by doping alkali element Na for Bi-site.[16] Compared with undoped sample, however, the magnetization of Na doped samples was reduced. On the other hand, Fe-site substitution by 3d transition metal (TM) ions might not only induce structure modifications to suppress the cycloidal spin structure but also the ferromagnetic interaction between Fe and 3d TM ions might further enhance the room temperature ferromagnetism. Recently, Zhao *et al.*[17] reported that the magnetization of $BiFe_{1-x}Ni_xO_3$ nanoparticles increases drastically with increasing Ni concentration. However, to data no single report is present on multiferroic properties of Na and Ni codoped $BiFeO_3$ nanoparticles.

In this paper, the $Bi_{0.97}Na_{0.03}Fe_{1-x}Ni_xO_3$ ($x = 0$, 0.005, 0.01, 0.015) nanoparticles were prepared via a facile sol-gel method. Detailed studies of structure, magnetic, electrical and optical properties of the samples were investigated. Due to charge neutrality, the substitution of divalent Ni^{2+} at trivalent Fe-site, can easily influence the number of holes and oxygen vacancies in samples. These defects can play an important role in the optical properties, because they produce the impurity band between the valence band and conduction band, which usually reduces the band gap.[16] In the Na and Ni codoped $BiFeO_3$ samples, the amount of oxygen vacancies and leakage current density are enhanced with the increase of Ni content. While interestingly, the band gap of samples first decreases for 0.5% Ni doping and then increases for 1.0% and 1.5% Ni doping. To explain this, a phenomenological qualitative model is proposed based on the electronic band gap. Additionally, at room temperature,

a)Authors to whom correspondence should be addressed. Electronic addresses: wfliu@tju.edu.cn and shouyu.wang@yahoo.com.

we have observed the intriguing threshold switching (TS) behavior when $x = 0.01$ and 0.015. To ascertain the presence of TS behavior, we introduce the conducting channel model based on the high-density mobile charges (e.g., oxygen vacancies).

EXPERIMENT

$Bi_{0.97}Na_{0.03}Fe_{1-x}Ni_xO_3$ ($x = 0$, 0.005, 0.01, 0.015) nanoparticles were synthesized by sol-gel method. Appropriate amounts of $Bi(NO_3)_3 \cdot 5H_2O$, $Fe(NO_3)_3 \cdot 9H_2O$, $NaNO_3$, and $Ni(NO_3)_2 \cdot 6H_2O$ were dissolved in ethylene glycol. Tartaric acid in 1:1 molar ratio with respect to metal cation was added to the solution, and the mixture was stirred at 70 °C for 3 h. The obtained solution was dried at 90 °C for 3 h until it was turned to yellowish-brown gel. The gel was further dried at 140 °C for 3 h, then annealed at 400 °C for 1.5 h, and finally ground into powders. Subsequently, the powders were calcined for 2 h at 550 °C to obtain samples.

The crystalline structure analysis of the samples was carried out by X-ray diffraction (XRD) (Rigaku D/MAX-2500 diffractometer with Cu Kα radiation). For the morphological study of nanoparticles, scanning electron microscopy (SEM) was carried out using MODEL SU8000 SERIES FIELD EMISSION SCANNING ELECTRON MICROSCOPE (User's Operation/Maintenance Edition). The average particle size and microstructural properties of the samples were investigated by transmission electron microscopy (TEM), high resolution transmission electron microscopy (HRTEM), and the corresponding selected area electron diffraction (SAED) pattern using JEM-2100F instrument. To analyze the oxygen vacancy concentration, X-ray photoelectron spectroscopy (XPS) was recorded with PHI1600. Magnetic characterization of the samples was measured on Magnetic Property Measurement System (MPMS) SQUID-VSM made by Quantum Design. UV-vis absorption spectrum of our nanoparticle samples was performed by Shimadzu UV-3600 UV-VIS-NIR spectrophotometer. To study the electrical properties, the samples were pressed into pellets by compaction of powders in a uniaxial press, and the pellets were sintered for half an hour at 550 °C. The dielectric properties were measured by a precise impendence analyzer WK 6400 with an ac signal of 1000 mV. The leakage current curve was evaluated using an Axiacct model TF 2000 ferroelectric analyser. All the measurements were carried out at room temperature.

RESULTS AND DISCUSSION

The Rietveld refinements were done on all the samples based on the XRD data to analyze the structural properties using FULLPROF software,[18] and the Rietveld refined XRD patterns are shown in Fig. 1. The XRD results indicate that all the main XRD diffraction peaks can be well fitted with the rhombohedral distorted perovskite (ABO_3) crystal structure with space group R3c. The obtained values of the lattice parameters for $Bi_{0.97}Na_{0.03}FeO_3$ are $a = b = 5.5755(7)$ Å and $c = 13.8510(1)$ Å, which are consistent with the reported values.[16] Detailed analysis of the structural parameters studied using the Rietveld refinement are given in Table I. It is evident from Table I that unit cell volume increases with Ni

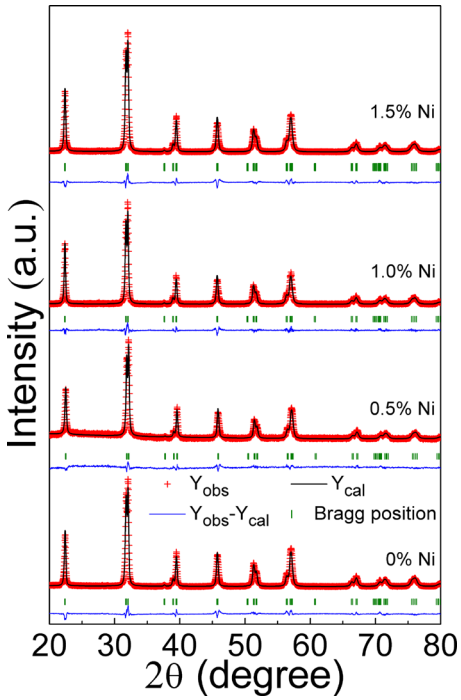

FIG. 1. Rietveld refined XRD pattern of $Bi_{0.97}Na_{0.03}Fe_{1-x}Ni_xO_3$ ($x = 0$, 0.005, 0.01, 0.015) nanoparticles at room temperature.

substitution, which is expected since the radius of Ni^{2+} ion (radius = 0.69 Å) is larger than that of the Fe^{3+} ion (radius = 0.645 Å).[19]

The typical TEM images of the $Bi_{0.97}Na_{0.03}FeO_3$ and 0.5% Ni doped $Bi_{0.97}Na_{0.03}FeO_3$ nanoparticles are shown in Fig. 2. From the TEM images, it is observed that the shapes of most particles are spherical, but some of them are irregular, and some agglomerations in nature are found. It can be seen in Figs. 2(a) and 2(b) that the average particle size of $Bi_{0.97}Na_{0.03}FeO_3$ and $Bi_{0.97}Na_{0.03}Fe_{0.995}Ni_{0.005}O_3$ samples lies between 40 and 60 nm. In addition, the SEM images of all samples show that the particle size has no significant difference, as shown in Fig. 3. The high resolution TEM (HRTEM) and the selected area electron diffraction (SAED) pattern obtained from an individual $Bi_{0.97}Na_{0.03}Fe_{0.995}Ni_{0.005}O_3$ nanoparticle are shown in the upper and lower insets of Fig. 2(b), respectively, which indicates the single-crystalline nature of our samples with a high degree of crystallinity.

The field dependent magnetization hysteresis (M-H) loops of the samples at room temperature are shown in Fig. 4. It can be clearly observed that all the samples show weak ferromagnetism at room temperature, which is quite different from the linear M-H relationship of bulk $BiFeO_3$. In bulk $BiFeO_3$, the magnetization at room temperature is suppressed

TABLE I. Structure parameters obtained from Rietveld refinement of $Bi_{0.97}Na_{0.03}Fe_{1-x}Ni_xO_3$ ($x = 0$, 0.005, 0.01, 0.015) samples.

x (%)	a (Å)	c (Å)	Unit cell volume (Å^3)	Fe-O-Fe
0	5.5755(7)	13.8510(1)	372.90	158.34°
0.5	5.5761(1)	13.8492(7)	372.93	156.54°
1.0	5.5764(8)	13.8518(7)	373.04	155.78°
1.5	5.5771(0)	13.8544(8)	373.20	155.77°

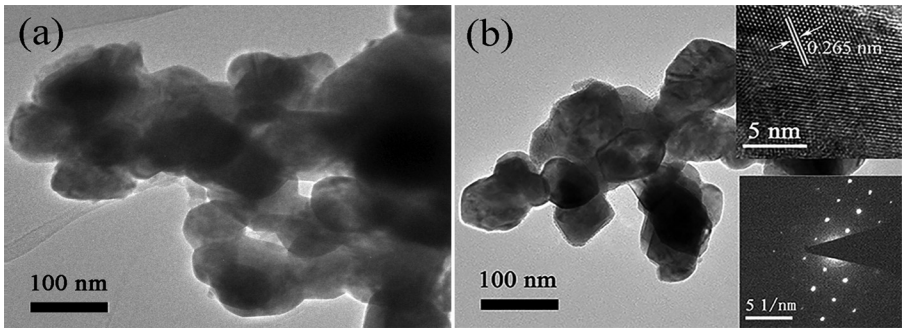

FIG. 2. TEM images of (a) $Bi_{0.97}Na_{0.03}FeO_3$ and (b) $Bi_{0.97}Na_{0.03}Fe_{0.995}Ni_{0.005}O_3$ nanoparticles.

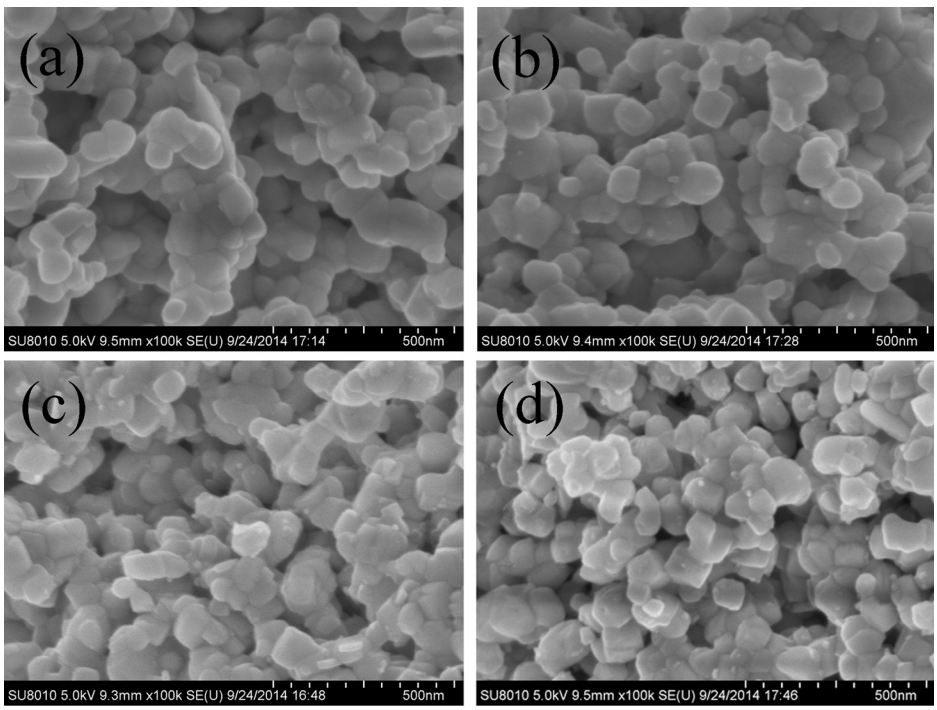

FIG. 3. SEM images of (a) $Bi_{0.97}Na_{0.03}FeO_3$, (b) $Bi_{0.97}Na_{0.03}Fe_{0.995}Ni_{0.005}O_3$, (c) $Bi_{0.97}Na_{0.03}Fe_{0.99}Ni_{0.01}O_3$, and (d) $Bi_{0.97}Na_{0.03}Fe_{0.985}Ni_{0.015}O_3$ samples.

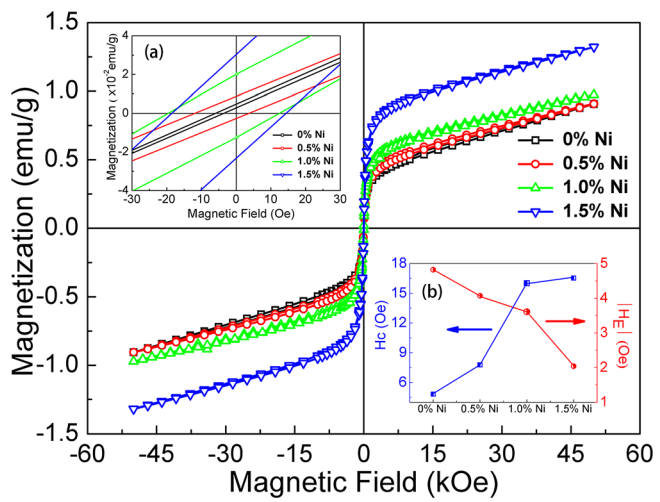

FIG. 4. The field dependent magnetization hysteresis (M-H) loops of $Bi_{0.97}Na_{0.03}Fe_{1-x}Ni_xO_3$ ($x = 0$, 0.005, 0.01, 0.015) nanoparticles at room temperature. Inset (a) the enlargement of M-H loops at magnetic field range from −30 Oe to +30 Oe. Inset (b) Ni concentration dependent coercive field and exchange bias field.

by a cycloidal spiral propagating along $[110]_{hex}$ with a period of 62 nm.[20] While in our nanoparticle system, the periodic spiral spin structure can be modified due to the reduction in the particle size. Therefore, the primary cause for the observed weak ferromagnetism in samples can be attributed to the size effect of the suppression of spiral order. Meanwhile, the G-type antiferromagnet can be described as comprising two spin sublattices with ferromagnetic interactions within one sublattice and antiferromagnetic interactions between sublattices.[9] In nanopaticle structures, the surface-to-volume ratio becomes very large, enhancing the tangible contribution to the particle's overall magnetization by incomplete compensation of two magnetic sublattices at the surface.[9] Thus, we conclude that uncompensated spins at the surface also contribute to the weak ferromagnetism. As can be seen from Fig. 4, with increasing Ni content, the magnetization increases significantly. Two major reasons could contribute to the enhancement of magnetization when the Ni is doped in the samples. Firstly, the increase in the magnetization of Ni substituted $Bi_{0.97}Na_{0.03}FeO_3$ may be attributed to the change

in the Fe-O-Fe bond angle. It is reported that the magnetization increases with decreasing Fe-O-Fe bond angle in $Bi_{1-x}Pr_xFeO_3$ nanoparticles and Dy-modified $BiFeO_3$ system.[21,22] In our $Bi_{0.97}Na_{0.03}Fe_{1-x}Ni_xO_3$ samples, the Rietveld refinements of XRD data (Table I) clearly reveal a decreasing trend in the Fe-O-Fe bond angle. Thus, Ni doping seems to induce more buckling in Fe-O-Fe bond angle, which in turn increases canting of spins and, hence, enhances the magnetization. Moreover, the change in electronic density of state distribution between Fe-O driven by the hybridization interaction is also responsible for the magnetization in $BiFeO_3$ system. Ryu *et al.*[23] reported that the Fe 3d-O 2p hybridization strength weakens with the reduced Fe-O-Fe bond angle in $BiFeO_3$ with rhombohedral symmetry, and they have further correlated the enhanced magnetization with the reduced degree of hybridization between Fe 3d and O 2p orbitals. The reduced Fe 3d-O 2p hybridization driven by the decreased Fe-O-Fe bond angle may could modulate the super-exchange interaction of Fe-O-Fe. So, the enhanced magnetization in our samples may also be related with the reduced degree of hybridization between Fe 3d-O 2p orbitals through the variation in the Fe-O-Fe bond angle. Secondly, the ferromagnetic exchange interaction between the neighboring Fe^{3+} and Ni^{2+} further enhances the magnetization in Ni doped $Bi_{0.97}Na_{0.03}FeO_3$ nanoparticles.[24]

The inset (a) of Fig. 4 shows the enlargement of M-H loops at magnetic field range from −30 Oe to +30 Oe. Interestingly, an obvious exchange bias effect of the samples was observed without any field cooling process. In the case of core-shell nanoparticles, the exchange bias may occur because of the coexisting antiferromagnetic and ferromagnetic components in the core and shell parts, respectively.[25] According to above described magnetic mechanism, in nanoparticle system, the uncompensated spins at the surface are ferromagnetic interactions, but the spins in the inner of nanoparticle are antiferromagnetism order, which can be represented as an AFM core and FM shell in nature.[16] Thus, the exchange bias can be interpreted by the presence of exchange coupling between the ferromagnetic surface and the antiferromagnetic core. From the inset (b) of Fig. 4, it can be seen the exchange bias field ($|H_E|$) is decreased and the coercivity (H_C) is increased with the increase of Ni concentration. The decrease of $|H_E|$ may be attributed to the decrease of interface exchange interaction due to the modulation of the uncompensated spins at the surface by Ni doping in the Fe-site. The main source of H_C for magnetic materials is shape anisotropy and magnetoelastic anisotropy in addition to the magnetocrystalline anisotropy.[26] For the present study, the nanoparticles are spherical in nature thus the contribution of shape anisotropy in H_C can be neglected. Therefore, the increase of H_C may be due to the enhancement of magnetocrystalline anisotropy and magnetoelastic anisotropy.

To analyze the oxygen vacancy concentration and the valence state of Fe, the XPS measurements were performed. Figures 5(a) and 5(b) show the XPS spectra analysis of the Fe 2p and O 1s core level regions by Lorentzian-Gaussian fitting for the samples, where the core level binding energies were aligned with respect to C 1s peak (284 eV). In Fig. 5(a),

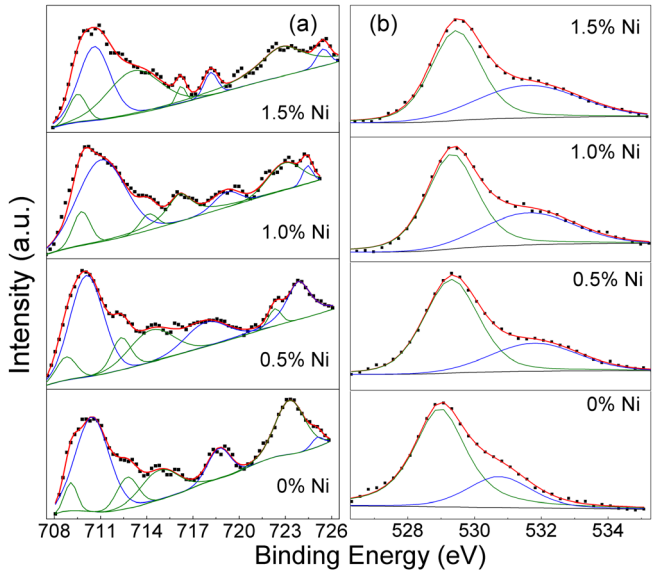

FIG. 5. (a) Fe 2p and (b) O 1s core levels XPS spectra for $Bi_{0.97}Na_{0.03}Fe_{1-x}Ni_xO_3$ ($x = 0$, 0.005, 0.01, 0.015) nanoparticles.

the Fe 2p spectra were fitted and the binding energy peak position of Fe $2p_{3/2}$ located at about 709.5 eV (olive line) is attributed to the Fe^{2+}; the position of Fe $2p_{3/2}$ located at about 710.4 eV (blue line) is ascribed to the Fe^{3+}. According to the fitting, the ratio of Fe^{2+}:Fe^{3+} is calculated as 10.4%, 13.7%, 14.9%, and 19.2% for $x = 0$, 0.005, 0.01, and 0.015, respectively, indicating the increase of Fe^{2+} ions with doping. In Fig. 5(b), the lower binding energy (olive line) located at about 529.5 eV and higher binding energy (blue line) located at about 531.5 eV are attributed to the oxygen present in the lattice and oxygen loss, respectively.[16] By calculating the ratio of area under the two peaks obtained from fitting the O 1s spectra, the results reveal that the oxygen vacancy concentration is effectively increased with increasing Ni content, which is consistent with those observed in other Ni doped BFO system.[24,27] It is well known that the substitution of divalent Ni^{2+} at trivalent Fe-site can easily increase the concentration of oxygen vacancy. The main processes can be described by the Kröger-Vink notions as follows:

In Ni doped samples, the hole ($h^{\bullet}$) is introduced directly to compensate the charge balance upon the doping of acceptor Ni, according to

$$NiO \rightarrow (Ni_{Fe})' + O_O^{\times} + h^{\bullet}. \quad (1)$$

And during the high temperature calcining process, the oxygen vacancy (V_O) is introduced by the following step:

$$O_O^{\times} \rightarrow V_O + \frac{1}{2}O_2. \quad (2)$$

Therefore, the more substitution of Fe^{3+} by Ni^{2+}, the more oxygen defects are produced.

In Fig. 6, the UV-vis absorption spectra of the samples were measured at room temperature. It can be observed that the samples can absorb considerable amount of visible light suggesting their potential application as visible-light photocatalyst. The optical band gap E_g for the samples can be

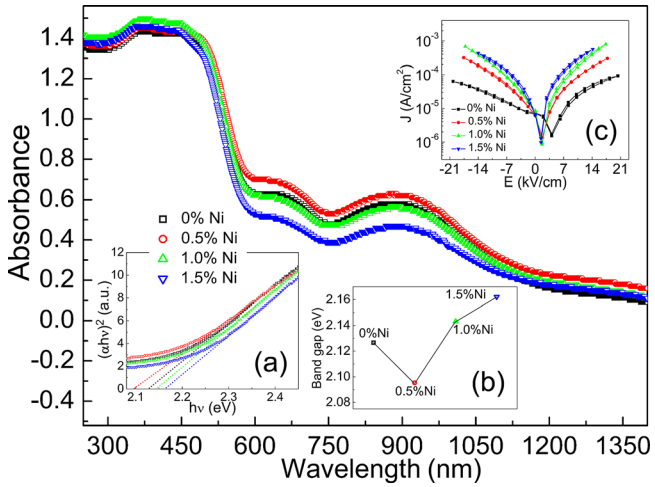

FIG. 6. UV-vis absorption spectrum of $Bi_{0.97}Na_{0.03}Fe_{1-x}Ni_xO_3$ ($x=0$, 0.005, 0.01, 0.015) nanoparticles. Inset (a) $(\alpha h\nu)^2$ versus $h\nu$ plot of samples. Inset (b) the band gap estimated from inset (a) is plotted as a function of x ($x=0$, 0.005, 0.01, 0.015). Inset (c) leakage current density (J) as a function of applied electric field (E) for the samples.

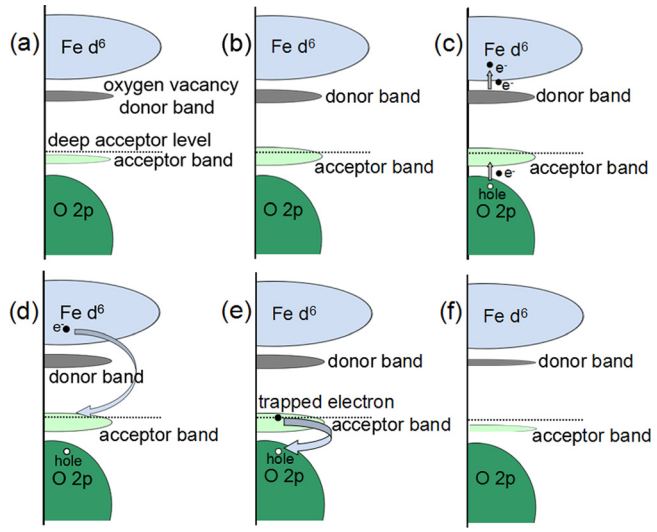

FIG. 7. The schematic diagram of the possible mechanism for electronic energy band.

calculated by the relation: $(\alpha h\nu)^2 = A(h\nu - E_g)$,[28] where A is a constant, $h\nu$ is the photon energy, E_g is the optical band gap, α is absorption coefficient. The corresponding plots of $(\alpha h\nu)^2$ versus $h\nu$ for $Bi_{0.97}Na_{0.03}Fe_{1-x}Ni_xO_3$ samples with $x=0$, 0.005, 0.01, 0.015 and the value of the band gap estimated by the linear extrapolation approach are shown in inset (a) and (b) of Fig. 6, respectively. The inset (c) of Fig. 6 shows the leakage current density (J) as a function of applied electric field (E) for all samples. It can be seen in inset (c) that the leakage current value increases with the increase of Ni content. The increase in leakage current density may be attributed to the increase of oxygen vacancy concentration. From the inset (b), it can be seen the band gap of $Bi_{0.97}Na_{0.03}FeO_3$ nanoparticles is estimated to be 2.12(7) eV which is quite comparable with recent report.[16] For the $Bi_{0.97}Na_{0.03}Fe_{1-x}Ni_xO_3$ nanoparticles with $x=0.005$, the band gap decreases to 2.09(5) eV. As reported, similar to many late 3d transition metal oxides, $BiFeO_3$ is a charge transfer-type material in which the conduction band is mainly composed of Fe 3d orbitals and the valence band is made of O 2p orbitals.[29] The oxygen vacancies reportedly lower than the Fe 3d levels energetically and result in a localized impurity band located below the conduction band minimum.[30] Thus, the decrease of band gap could be attributed to the increase of oxygen vacancy impurity band. While interestingly, with further doping ($x=0.01$, 0.015), the band gap is slightly increased (2.14(3) eV, 2.16(2) eV for 1%, 1.5% Ni doped samples, respectively), meanwhile, the leakage current density and oxygen vacancy of samples also are significantly increased.

To better understand the increase of leakage current density and meanwhile the increase of band gap with increasing Ni content, a phenomenological qualitative model is introduced. A schematic diagram of the possible mechanism for electronic energy band is shown in Fig. 7. At per Ni^{2+} substituted Fe^{3+}-site, there is one valence electron deficient to coordinate with contiguous oxygen. The hole ($h^{\bullet}$) is produced in this process, and the main process can be described by the Eq. (1). In the schematic diagram, the hole as an acceptor band locates the top of valence band and the oxygen vacancy (V_O) impurity band locates at the bottom of conduction band as a kind of donor level. Accordingly, the band gap of $Bi_{0.97}Na_{0.03}Fe_{0.995}Ni_{0.005}O_3$ could also become narrow due to the created holes. As discussed above, however, with further doping ($x=0.01$, 0.015), the band gap is increased. Based on the semiconductor theory, with the further increase of Ni content, more holes are formed which results in a wider acceptor band, and some holes of wider acceptor band may locate at deep acceptor level, as shown in Fig. 7(b). The holes locating at deep level may act as recombination centers which could increase the recombination rate of the electron-hole pairs, and eventually narrow the oxygen vacancy (V_O) donor band and acceptor band. In fact, the recombination process can be separated into two steps: (1) the electrons in the valence band are excited into acceptor band, which leads to the forming of the free holes in valence band, meanwhile, the electrons in the oxygen vacancy (V_O) donor band could be introduced into conduction band due to the thermal excitation (as shown in Fig. 7(c)); and (2) the conduction band electrons caused by the ionization of oxygen vacancies can combine with the holes at recombination centers (as shown in Fig. 7(d)), and the trapped electrons are unstable and will subsequently recombine with holes in the valence band generated from step (1) (as shown in Fig. 7(e)). Thus overall, the holes in the acceptor band recombine with electrons in the oxygen vacancy (V_O) donor band, which eventually narrow the oxygen vacancy (V_O) donor band and acceptor band thus increases the band gap, as shown in Fig. 7(f). As a consequence of ionization, neutral oxygen vacancies (V_O) release one or two electrons and become positively charged oxygen vacancies ($V_O^{\bullet}$ or $V_O^{\bullet\bullet}$), as described by

$$V_O \rightarrow V_O^{\bullet} + e', \tag{3}$$

$$V_O^{\bullet} \rightarrow V_O^{\bullet\bullet} + e'. \tag{4}$$

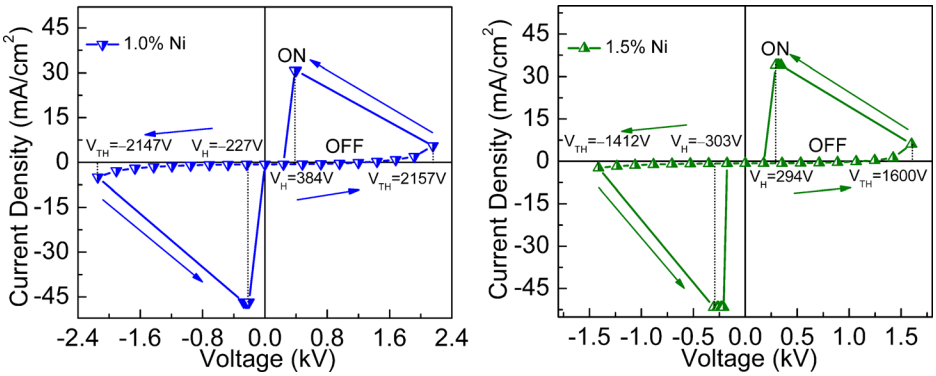

FIG. 8. The threshold switching (TS) behaviors in $Bi_{0.97}Na_{0.03}Fe_{1-x}Ni_xO_3$ ($x = 0.01, 0.015$) samples.

These ionized oxygen vacancies can move through the sample under electric fields to find a new thermodynamic equilibrium, which is known to produce the leakage current density in samples.[9,30] Thus, we conclude that the increase in leakage current density can be attributed to the increase of oxygen vacancy concentration.

The J-V curves of $Bi_{0.97}Na_{0.03}Fe_{1-x}Ni_xO_3$ ($x = 0$, 0.005, 0.01, 0.015) samples were further measured under different applied voltage, and the intriguing threshold switching (TS) behavior was observed in 1% and 1.5% Ni doped samples when the applied voltage increased to a specific value. The nearly symmetric TS behaviors are shown in Fig. 8. As can be seen from each J-V curve, in sweeping range from $0 \sim V_{TH}$, the threshold switching appears as an ohmic, high resistance connection between the cathode and anode electrodes. The current density increases with the applied voltage, first linearly then non-linearly, until the threshold voltage (V_{TH}) is achieved, at which point the device (Ag/$Bi_{0.97}Na_{0.03}Fe_{1-x}Ni_xO_3$/Ag "Sandwich" structure) switches rapidly into a highly conducting state (shown as the ON state). In ON state, as the applied voltage is decreased, the device rapidly switches back to its initial high resistance state (shown as the OFF state) at holding voltage (V_H). The electric-field-induced TS behavior instead of common J-V characteristic was firstly discovered in chalcogenide glasses by Ovshinsky in 1968.[31] After the publication of Ovshinsky's paper, a lot of studies on TS behavior in amorphous semiconductor, such as Sb_xSe_{1-x}, $Ge_2Sb_2Te_5$, and $Te_{48}As_{30}Si_{12}Ge_{10}$, were investigated.[32–34] Furthermore, TS has also been observed in transition metal-oxide materials, such as NiO and Fe_2O_3 systems.[35,36] However, the TS phenomenon as an important electrical field controlled switching effect is rarely reported in $BiFeO_3$ nanoparticle system.

So far, some possible mechanisms for the observed TS effect have been discussed for various chalcogenide amorphous semiconductors systems. Such as, the Adler model envisioned the TS event to result from a process of high field carrier generation leading to trap filling and saturation of the carrier recombination process.[37] In 2008, Ielmini proposed another TS model, and it builds on a new interpretation of the subthreshold conduction process.[38] In a report by Ovshinsky *et al.*,[39] the switching mechanism in semiconducting glasses was considered as a thermal origin from Joule heating. However, the mechanism of the TS behavior still remains unclear, and further research is necessary. In our samples, the substitution of aliovalent element produces more oxygen vacancy, which was obtained from the XPS results. It is reported that the oxygen vacancies play an important role in I-V behaviors of $BiFeO_3$ system.[30,40,41] Thus, we suspect that the TS behaviors observed in $Bi_{0.97}Na_{0.03}Fe_{1-x}Ni_xO_3$ ($x = 0.01$, 0.015) samples may be related to high-density mobile charges (e.g., oxygen vacancies). Under the lower applied voltage, oxygen vacancies are relatively decentralized. Once a sufficiently applied high voltage (V_{TH}) is reached, the ionized oxygen vacancies ($V_O^{\bullet}$ or $V_O^{\bullet\bullet}$) are able to migrate quickly and form a conducting path, which results in an enhanced conductance state, i.e., ON state, as shown in Fig. 9(a). In the ON state, the high current flowing through the high conducting path generates a lot of heat. Thus, when the bias voltage decreases below the holding voltage (V_H), the ionized oxygen vacancies can be thermally activated to the original evenly distributed state due to relatively lower degree of electric field strength. So, the device switches to the initial high resistance state (OFF state), as shown in

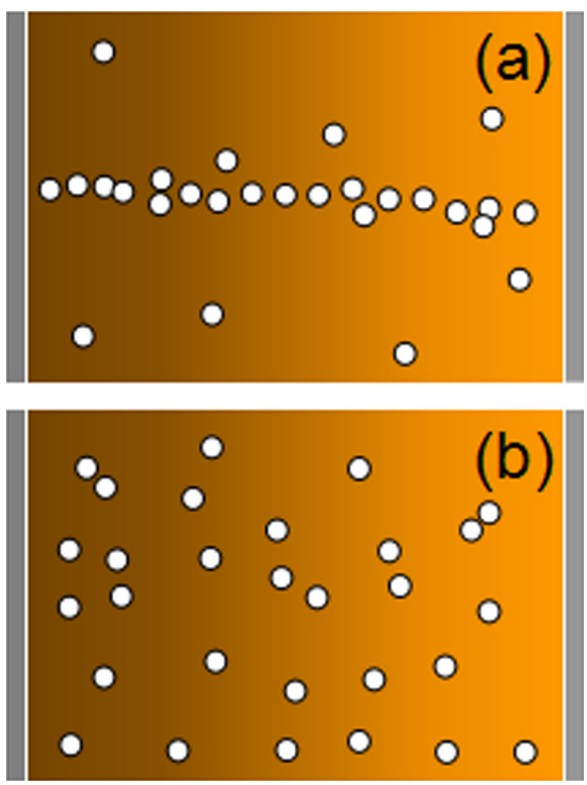

FIG. 9. Schematic diagram describing the possible mechanism of TS behavior in $Bi_{0.97}Na_{0.03}Fe_{1-x}Ni_xO_3$ ($x = 0.01$, 0.015) samples.

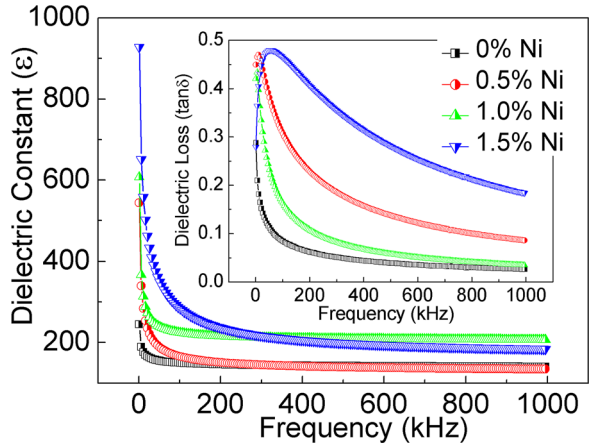

FIG. 10. The dielectric constant of $Bi_{0.97}Na_{0.03}Fe_{1-x}Ni_xO_3$ ($x=0$, 0.005, 0.01, 0.015) samples at room temperature. The inset shows the dielectric loss of all samples.

Fig. 9(b). With the increase of Ni content, oxygen vacancies increased, which makes the formation of conducting path easier, thus V_{TH} decreases (as shown in Fig. 8).

Figure 10 and the inset show the frequency (f) dependence of dielectric constant (ε) and dielectric loss ($\tan\delta$) of the $Bi_{0.97}Na_{0.03}Fe_{1-x}Ni_xO_3$ ($x=0$, 0.005, 0.01, 0.015) samples, respectively. The dielectric constants of all samples are decreased drastically with the increase of frequency in low-frequency region, called the f-sensitive region and then tend to be constant when the frequency reaches a certain value (the f-stable region). This phenomenon can be understood from the Maxwell-Wagner model related to the space charge relaxation.[42] At low frequencies, the space charges (e.g., oxygen vacancies) are able to follow the frequency of the applied field, whereas the space charges do not find time to undergo relaxation at high frequency region.[43] Thus, the dielectric constant is observed to decrease with the increase of frequency. Compared with undoped sample, the ε decreases even faster in low-frequency region with the increase of Ni content. This may be in connection with the variations in the concentration of oxygen vacancies, which is in accordance with the above analyses of O 1s XPS spectra and leakage current density. A increase in dielectric loss has been observed in the inset of Fig. 10 with the increase of Ni concentration and when the concentration of Ni is 1.5%, the dielectric loss is the largest.

CONCLUSIONS

In summary, Na and Ni codoped $BiFeO_3$ nanoparticles have been synthesized by a sol-gel method. Through M-H measurements, it is observed that the samples show a weak ferromagnetic nature, which is due to the suppression of spiral order and the contribution of uncompensated spins at the surface of particles. The exchange bias phenomenon is observed without any field cooling process for the samples, which can be attributed to the core (AFM)-shell (FM) structure. However, Ni doping makes the exchange bias phenomenon less obvious. With the increase of Ni content, the leakage current density is enhanced due to the increase of oxygen vacancies, whereas the band gap first decreases for 0.5% Ni doping and then increases for 1.0% and 1.5% Ni doping. To explain this, a phenomenological qualitative model is introduced based on the interplay of oxygen vacancy donor and hole acceptor. Additionally, the intriguing threshold switching (TS) behavior is observed in 1% and 1.5% Ni doped samples at room temperature, which may be related to the high-density mobile charges such as oxygen vacancies ($V_O^{\bullet}$ or $V_O^{\bullet\bullet}$), and is explained by a conducting channel model.

ACKNOWLEDGMENTS

This work was funded by the National Natural Science Foundation of China (Project Nos. 11004148 and 11104202), the Research Grant Council of Hong Kong (Project Nos. HKU 702112P and RGC 70181), and the Guangxi Natural Science Foundation (Grant No. 2012GXNSFGA060002).

[1]W. Eerenstein, N. D. Mathur, and J. F. Scott, Nature **442**, 759 (2006).
[2]S. W. Cheong and M. Mostovoy, Nature Mater. **6**, 13 (2007).
[3]A. Singh, V. Pandey, R. K. Kotnala, and D. Pandey, Phys. Rev. Lett. **101**, 247602 (2008).
[4]G. Catalan and J. F. Scott, Adv. Mater. **21**, 2463 (2009).
[5]J. Wang, J. B. Neaton, H. Zheng, V. Nagarajan, S. B. Ogale, B. Liu, D. Viehland, V. Vaithyanathan, D. G. Schlom, U. V. Waghmare, N. A. Spaldin, K. M. Rabe, M. Wuttig, and R. Ramesh, Science **299**, 1719 (2003).
[6]C. Ederer and N. A. Spaldin, Phys. Rev. B **71**, 060401 (2005).
[7]K. Y. Yun, M. Noda, and M. Okuyama, J. Korean Phys. Soc. **42**, 1153 (2003).
[8]F. Gao, Y. Yuan, K. F. Wang, X. Y. Chen, F. Chen, J. M. Liu, and Z. F. Ren, Appl. Phys. Lett. **89**, 102506 (2006).
[9]T. J. Park, G. C. Papaefthymiou, A. J. Viescas, A. R. Moodenbaugh, and S. S. Wong, Nano Lett. **7**, 766 (2007).
[10]Q. Y. Xu, H. F. Zai, D. Wu, T. Qiu, and M. X. Xu, Appl. Phys. Lett. **95**, 112510 (2009).
[11]J. Liu, L. Fang, F. G. Zheng, S. Ju, and M. R. Shen, Appl. Phys. Lett. **95**, 022511 (2009).
[12]W.-H. Kim and J. Y. Son, Appl. Phys. Lett. **103**, 132907 (2013).
[13]Z. X. Cheng, A. H. Li, X. L. Wang, S. X. Dou, K. Ozawa, H. Kimura, S. J. Zhang, and T. R. Shrout, J. Appl. Phys. **103**, 07E507 (2008).
[14]V. A. Khomchenko, D. A. Kiselev, I. K. Bdikin, V. V. Shvartsman, P. Borisov, W. Kleemann, J. M. Vieira, and A. L. Kholkin, Appl. Phys. Lett. **93**, 262905 (2008).
[15]P. Suresh and S. Srinath, J. Appl. Phys. **113**, 17D920 (2013).
[16]H. Zhang, W. F. Liu, P. Wu, X. Hai, M. C. Guo, X. J. Xi, J. Gao, X. Wang, F. Guo, X. L. Xu, C. Wang, G. Y. Liu, W. G. Chu, and S. Y. Wang, Nanoscale **6**, 10831 (2014).
[17]J. G. Zhao, X. H. Zhang, S. J. Liu, W. Y. Zhang, and Z. J. Liu, J. Alloy. Compds. **557**, 120 (2013).
[18]A. Tamilselvan, S. Balakumar, M. Sakar, C. Nayek, P. Murugavel, and K. S. Kumarc, Dalton Trans. **43**, 5731 (2014).
[19]J. S. Park, Y. J. Yoo, J. S. Hwang, J.-H. Kang, B. W. Lee, and Y. P. Lee, J. Appl. Phys. **115**, 013904 (2014).
[20]P. Chen, Ö. Günaydın-Şen, W. J. Ren, Z. Qin, T. V. Brinzari, S. McGill, S.-W. Cheong, and J. L. Musfeldt, Phys. Rev. B **86**, 014407 (2012).
[21]K. Prashanthi, B. A. Chalke, K. C. Barick, A. Das, I. Dhiman, and V. R. Palkar, Solid State Commun. **149**, 188 (2009).
[22]S. K. Srivastav, N. S. Gajbhiye, and A. Banerjee, J. Appl. Phys. **113**, 203917 (2013).
[23]S. Ryu, J.-Y. Kim, Y.-H. Shin, B.-G. Park, J. Y. Son, and H. M. Jang, Chem. Mater. **21**, 5050 (2009).
[24]Y. J. Yoo, J. S. Hwang, Y. P. Lee, J. S. Park, J.-H. Kang, J. Kim, W. Lee, and M. S. Seo, J. Appl. Phys. **114**, 163902 (2013).
[25]S. M. Yusuf, P. K. Manna, M. M. Shirolkar, S. K. Kulkarni, R. Tewari, and G. K. Dey, J. Appl. Phys. **113**, 173906 (2013).
[26]K. Chakrabarti, K. Das, B. Sarkar, S. Ghosh, S. K. De, G. Sinha, and J. Lahtinen, Appl. Phys. Lett. **101**, 042401 (2012).
[27]X. Qi, J. Dho, R. Tomov, M. G. Blamire, and J. L. MacManus-Driscoll, Appl. Phys. Lett. **86**, 062903 (2005).

[28]J. Tauc, *Amorphous and Liquid Semiconductors* (Plenum Press, New York, 1974), p. 171.
[29]K. K. Bharathi, W.-M. Lee, J. H. Sung, J. S. Lim, S. J. Kim, K. Chu, J. W. Park, J. H. Song, M.-H. Jo, and C.-H. Yang, Appl. Phys. Lett. **102**, 012908 (2013).
[30]C.-H. Yang, J. Seidel, S. Y. Kim, P. B. Rossen, P. Yu, M. Gajek, Y. H. Chu, L. W. Martin, M. B. Holcomb, Q. He, P. Maksymovych, N. Balke, S. V. Kalinin, A. P. Baddorf, S. R. Basu, M. L. Scullin, and R. Ramesh, Nature Mater. **8**, 485 (2009).
[31]S. Ovshinsky, Phys. Rev. Lett. **21**, 1450 (1968).
[32]E. H. Aly and A. M. Ibrahim, J. Phys. D: Appl. Phys. **33**, 2549 (2000).
[33]J. Bae, I. Hwang, Y. Jeong, S.-O. Kang, S. Hong, J. Son, J. Choi, J. Kim, J. Park, M.-J. Seong, Q. Jia, and B. H. Park, Appl. Phys. Lett. **100**, 062902 (2012).
[34]S. Hudgens, Phys. Status Solidi B **249**, 1951 (2012).
[35]C. Wang, K. J. Jin, Z. T. Xu, L. Wang, C. Ge, H. B. Lu, H. Z. Guo, M. He, and G. Z. Yang, Appl. Phys. Lett. **98**, 192901 (2011).
[36]J. Y. Lee, Y. J. Baek, Q. Hu, Y. J. Choi, C. J. Kang, H. H. Lee, H. M. Kim, K. B. Kim, and T. S. Yoon, Appl. Phys. Lett. **102**, 122111 (2013).
[37]D. Adler, H. K. Henisch, and N. F. Mott, Rev. Mod. Phys. **50**, 209 (1978).
[38]D. Ielmini, Phys. Rev. B **78**, 035308 (2008).
[39]K. W. Böer and S. R. Ovshinsky, J. Appl. Phys. **41**, 2675 (1970).
[40]K. Yin, M. Li, Y. Liu, C. He, F. Zhuge, B. Chen, W. Lu, X. Pan, and R. Li, Appl. Phys. Lett. **97**, 042101 (2010).
[41]Y. Shuai, S. Zhou, C. Wu, W. Zhang, D. Burger, S. Slesazeck, T. Mikolajick, M. Helm, and H. Schmidt, Appl. Phys. Express **4**, 095802 (2011).
[42]C. Elissalde and J. Ravez, J. Mater. Chem. **11**, 1957 (2001).
[43]H. O. Rodrigues, G. F. M. Pires Junior, J. S. Almeida, E. O. Sancho, A. C. Ferreira, M. A. S. Silva, and A. S. B. Sombra, J. Phys. Chem. Solids **71**, 1329 (2010).